Pergamon

Bioorganic & Medicinal Chemistry 10 (2002) 3135–3143

BIOORGANIC & MEDICINAL CHEMISTRY

Synthesis, Biological Activity and Receptor-Based 3-D QSAR Study of 3′-*N*-Substituted-3′-*N*-debenzoylpaclitaxel Analogues

Eun Joo Roh,[a,b] Deukjoon Kim,[b,*] Jun Yong Choi,[c] Bon-Su Lee,[c,*] Chong Ock Lee[d] and Choong Eui Song[a,*]

[a]*Life Sciences Division, Korea Institute of Science and Technology, PO Box 131, Cheongryang, Seoul, 130-650, Republic of Korea*
[b]*College of Pharmacy, Seoul National University, Shinrim-Dong, Kwanak-ku, Seoul, 152-742, Republic of Korea*
[c]*Department of Chemistry, Inha University, Yonghyun-Dong 253, Nam-ku, Inchon, 402-751, Republic of Korea*
[d]*Screening Center, Korea Research Institute of Chemical Technology, PO Box 107, Yusong, Daejeon, 305-606, Republic of Korea*

Received 18 March 2002; accepted 10 June 2002

Abstract—3′-*N*-Substituted-3′-*N*-debenzoylpaclitaxel analogues were synthesized and investigated for their 3-D QSAR by using comparative molecular field analysis (CoMFA). The CoMFA model obtained from receptor(microtubule)–paclitaxel binding structure displays an excellent predictive power to forecast the biological activity of new 3′-*N*-substituted-3′-*N*-debenzoylpaclitaxel analogues as well as the ability to explain the activity of the known paclitaxel analogues. The cross-validated r^2_{cv} values of the selected models are 0.835 and 0.616 for A549 and SK-OV-3, respectively, and the non-cross-validated r^2_{ncv} values of them are 0.992 and 0.974.

Introduction

Paclitaxel (Taxol®), a highly functionalized diterpene originally isolated from the pacific yew (*Taxus brevifolia*), has been proven to be one of the most promising antitumor compounds of the decade.[1] Due to its unique and effective mode of action,[2–4] paclitaxel exhibits impressive activity against various types of cancers, especially breast, ovarian, germ cell, lung, and esophageal cancers, that have not been effectively treated by other conventional anticancer agents.[5] To date, numerous analogues have been prepared to develop new taxoids with improved activity and decreased side effects.[6] Although a large body of paclitaxel structure–activity relationships (SARs)[7–9] has been generated, a detailed investigation on paclitaxel analogues having 3′-*N*-substituent of similar size with 3′-*N*-benzoyl group has received little attention. In the course of our SAR study of taxoids, we recently found that replacement of phenyl group of 3′-*N*-benzoyl with some aliphatic groups such as cyclopentyl (**1p**), 1-cyclopentenyl (**1k**), cyclohexyl (**1u**) and 1-cyclohexenyl (**1j**) gave equally or more active compounds.[10] In particular, the analogues bearing cycloalkenyl groups were up to 20 times more potent than paclitaxel. These preliminary results intrigued us to carry out more detailed SAR study at the 3′-*N*-position.[20] Here we report synthesis, biological activity and receptor-based 3-D QSAR study of 3′-*N*-substituted-3′-*N*-debenzoyl-paclitaxel analogues. The CoMFA model obtained from receptor(microtubule)-paclitaxel binding structure displayed an excellent predictive power to forecast the biological activity of new 3′-*N*-substituted-3′-*N*-debenzoylpaclitaxel analogues as well as the ability to explain the activity of the known paclitaxel analogues.

Results and Discussion

Biological activity

The biological activities of 3′-*N*-debenzoyl-3′-*N*-substituted paclitaxel analogues **1a**–**x** prepared by our reported protocol[10,19,20] were evaluated for their cytotoxicities against human cancer cell lines, A 549 (non-small cell lung carcinoma) and SK-OV-3 (ovarian carcinoma), by SRB assay.[11,12] Since a log transform of the biological data usually removes much of

*Corresponding authors. Tel.: +82-2-958-5143; fax: +82-2-958-5189; e-mail: s1673@kist.re.kr

0968-0896/02/$ - see front matter © 2002 Elsevier Science Ltd. All rights reserved.
PII: S0968-0896(02)00217-1

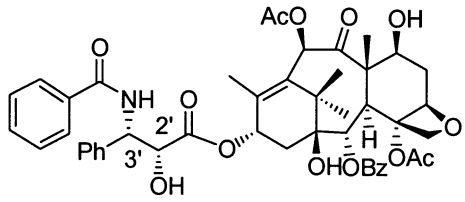

Paclitaxel

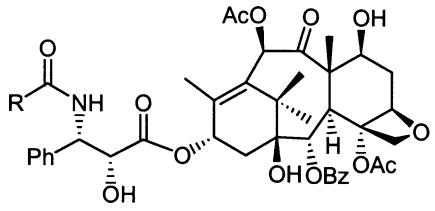

1a-x

the skewness in the data, the quantitative measure of biological potency in classic QSAR as well as 3-D QSAR is normally defined as log(1/C) where C is the molar concentration of drug producing a standard response (ED_{50}). As shown in Table 1, the anticancer activity was largely influenced by small change of the structure of 3′-*N*-substituents. For example, 3,3′-dimethylacryloyl (**1a**), *trans*-crotonyl (**1b**), 2-butynoyl (**1q**) and *trans*-2-hexenoyl (**1x**) substituted analogues showed up to 2 orders of magnitude stronger activity than paclitaxel. The analogues bearing *N*-cycloalkene carbonyl, cycloalkane carbonyl group were almost same or up to 20 times more potent than paclitaxel. However, the alkoxycarbonyl (**1w**) and alkenoxycarbonyl (**1i** and **1l**) substituted analogues showed much lower activity. With these broad distribution of activities of 3′-*N*-substituted-3′-*N*-debenzoylpaclitaxel analogues, we tried to build up CoMFA model based on the receptor–ligand complex.

Determination of CoMFA model and application to test set

In the case of paclitaxel, it was very difficult to constitute training set due to the several conformers by the presence of many rotatable bonds at C-13 side chain. The results of CoMFA[13] analysis with each selected structure were very different due to the existence of various plausible conformers. To alleviate these shortcomings, alternative approach called structure-based 3-D-QSAR technique[14] was applied in this research. A three-dimensional quantitative structure–activity relationship (3-D-QSAR) for paclitaxel derivatives was obtained by applying comparative molecular field analysis (CoMFA). The bioactive conformation of a drug molecule refers to the conformation bound to its target receptor. Therefore, the reliability of CoMFA results depends on the establishment of the bioactive conformation. The X-ray structure (1TUB)[15] of docetaxel-bound microtubule available in Brookhaven Protein Data Bank was used in order to determine the bioactive conformers of paclitaxel and its derivatives. For the construction of CoMFA field, 2 and 1 Å grid interval region partial least-squares analysis (PLS) was done. In 2 Å grid space, CoMFA field was composed of 3187 descriptors with Tripos Standard CoMFA field. In 1 Å grid space, the same procedure was conducted on 12167 descriptors. From 2 and 1 Å grid intervals, 12 CoMFA fields were obtained after applying region focusing method.[16] And then, the cross-validation r^2 was calculated with changing column filtering values

Table 1. In vitro anticancer activity [$-\log(ED_{50}/ED_{50(paclitaxel)})$] of 3′-*N*-modified taxoids

	Taxoid [RC(O)–]	Observed value A549	Observed value SK-OV-3	Predicted value A549	Predicted value SK-OV-3
Paclitaxel	Benzoyl	0	0	−0.19	−0.40
1a	3, 3′-Dimethylacryloyl	2.10	1.3	2.25	1.14
1b	*trans*-Crotonyl	2.10	0.74	2.01	0.78
1c	Cyclopropanecarbonyl	0.41	−0.39	0.34	−0.22
1d	Cyclobutanecarbonyl	−0.07	−0.68	−0.18	−0.73
1e	*p*-Fluorobenzoyl	−1.46	−1.58	−1.60	−1.68
1f	*p*-Nitrobenzoyl	−2.30	−1.86	−2.35	−1.90
1g	*p*-Iodobenzoyl	−1.60	−2.35	−1.55	−2.27
1h	*trans*-2-Methyl-2-butenoyl	0	−0.7	0.14	−0.39
1i	Isopropenyloxycarbonyl	−1.04	−1.74	−1.13	−1.70
1j	1-Cyclohexenecarbonyl	0.25	0.08	0.50	0.22
1k	1-Cyclopentenecarbonyl	1.30	0.89	1.34	0.88
1l	Vinyloxycarbonyl	−2.00	−2	−1.73	−1.63
1m	Acryloyl	−1.03	−0.97	−1.08	−0.59
1n	1-Methyl-2-cyclohexenecarbonyl	−1.90	−1.88	−1.82	−1.85
1o	*trans*-2-Pentenoyl	−2.00	−2	−1.91	−1.93
1p	Cyclopentanecarbonyl	0.40	−0.22	0.47	−0.16
1q	2-Butynoyl	1.17	0.01	1.03	0.07
1r	4-Pentynoyl	−2.60	−2	−2.54	−2.33
1s	Propiolyl	−1.00	0.2	−1.02	−0.21
1t	Phenylpropiolyl	−0.78	−0.76	−0.72	−0.63
1u	Cyclohexanecarbonyl	−0.65	−0.75	−0.84	−0.63
1v	*trans*-2-Ethyl-2-hexenoyl	−1.59	−1.78	−1.65	−1.99
1w	Isobutyloxycarbonyl	−0.51	−0.91	−0.56	−1.06
1x	*trans*-2-Hexenoyl	2.08	1.22	2.07	1.08

and non-cross-validation r^2 was done with the same used descriptors. Six PLS results with high r^2_{cv} and r^2_{ncv} values were regarded as good models for A549, and four PLS results for SK-OV-3. To choose the best model from these ones, leave-50%-out and leave-20%-out procedures were applied. These cross-validation techniques have been shown to yield better indices for the robustness of a model than the normal leave-one-out method because the latter might lead to high r^2_{cv} values which do not necessarily reflect a general predictiveness of a model. After running iteratively, each best predictive model with the highest r^2_{cv} value was selected. These procedures used for best predictive model build-up were applied to two cell lines, A549 and SK-OV-3. The details of these procedures were described in experimental section and the standard parameters of best predictive model were summarized in Table 2. Graphs shown in Figure 1 demonstrate the relationship of actual activities and calculated values for the best predictive models of two cell lines, A549 and SK-OV-3, respectively. The cross-validation r^2_{cv} values of the best predictive models for A549 and SK-OV-3 were 0.835 and 0.616 using five optimum number of components. And the non-cross-validation r^2_{ncv} values for them were 0.992 and 0.974 with standard error of estimation (SEE) of 0.137 and 0.199, respectively. These models were also robust, indicated by a high r^2_{cv} values (0.521, 0.740 for A549 and 0.595, 0.700 for SK-OV-3 cell lines) obtained by using the leave-50%-out and leave-20%-out procedures.[17] The derived CoMFA model can be used to predict the activity of new compounds in the hope of increasing the desired biological activity. As a precedent of it, we applied the derived CoMFA models to test set. From these application results (Table 3), the selected models for each cell line were clarified as the best predictive models.

Table 2. Statistic of the best predictive CoMFA Model for A549 and SK-OV-3 cells

	A549	SK-OV-3
Number of compounds	25	25
The name of selected CoMFA Model[a]	CF1_SD05[i]	CF1_SD05
Column filtering value[b]	0.6	0.9
Number of used descriptors[c]	734	641
Optimum number of components	5	4
R^2_{cv}[d]	0.835	0.739
R^2_{ncv}[e]	0.992	0.974
Standard error of estimate	0.137	0.228
F values[f]	496.960	133.025
$R^2_{l50\%o}$[g]	0.632	0.595
$R^2_{l20\%o}$[h]	0.788	0.700

[a]Selected best predictive models after applying region focusing method, various column filtering values and leave-50%-out and leave-20%-out techniques.
[b]The values of 0.5∼2.0 kcal/mol were used to omit lattice points whose energy variance is less than defined values.
[c]The number was resulted not from user defining but from the column filtering method.
[d]Crossvalidated standard error of estimate(s) = (PRESS/($n-c-1$))1/2, n = number of rows, c = number of components, PRESS = $\Sigma(Y_{predicted} - Y_{actual})$.
[e]Non-crossvalidated $r^2 = 1.0-(\Sigma Ypred - Yactual)^2/(\Sigma Yactual - Ymean)^2$.
[f]The ration of r^2 to $1.0-r^2$(explained to unexplained).
[g]The average value of r^2_{cv} after 12 times of leave-50%-out calculation.
[h]The average value of r^2_{cv} after twelve times of leave-20%-out calculation.
[i]CF1_SD05 means that CoMFA Field with 1 Å grid interval was analyzed at first, and then region focusing method was applied with the weighting function of SD*Coefficients and with exponential factor of 0.5 from the good PLS result of it.

Binding site interactions of paclitaxel and microtubule

As a consequence of conformational analysis of receptor binding paclitaxel complex, specific binding site interactions were also determined. As shown in Figure 2, the modified R group on 3′-*N*-position was not involved in specific binding with receptor. Other researchers[18] mentioned that the stereochemistry of 2′-OH is deeply associated with the binding of paclitaxel and microtubule. This is also confirmed in this research. 2′-OH group and 2-benzoyl group are participated in hydrogen bonding with ARG369 and ARG278, respectively. The oxygen of 3′-carbonyl is expected to bind weakly with SER25, VAL23 and HIS229; 3.69, 2.76 and 2.58 Å. Since these distances are rather longer than those of normal hydrogen bonding, it is assumed that these residues act as immobilizing R group and positioning it. From these results, the orientation of the R part is from inner to outer of active site.

CoMFA contour maps

The CoMFA steric and electrostatic fields from the best predictive model (CF1_StD05) were plotted as three-dimension colored contour maps in Figures 3 (steric field maps) and 4 (electrostatic field maps). The steric field has more contribution to predict activity than the electrostatic field; 79.0 and 21.0% for A549 cell line, 79.6 and 20.4% for SK-OV-3 cell line, respectively. In Figure 3, green contours represent regions where bulky groups are favorable to the activity and yellow ones describe regions where bulky groups are unfavorable. There are no significant differences in maps of both cell lines, which can be attributed to similar trend of activity for both cell lines. This is also shown in Figure 4 in which the blue and the red contours represent regions where the more positively charged groups and the more negatively charged groups are favorable to enhance activities, respectively. As shown in Figure 3, there is a sterically favored region below the dimethylacryloyl group. It means there is a possibility to increase the activity by occupying this area. As shown above, the contribution of steric factor is about 4 times higher than that of electronic factor, so instead of changing electronic property, occupying sterically favored region would be helpful for the development of more potent analogues.

Experimental

Synthesis of analogues

General methods. Chromatographic purification of products was carried out by flash chromatography using Merck silica gel 60 (230–400 mesh). Thin layer chromatography was carried out on Merck silica gel 60F plates. ^{1}H NMR (300 MHz) and ^{13}C NMR (75.0 MHz) spectra were recorded on a Varian Gemini 300 spectrometer

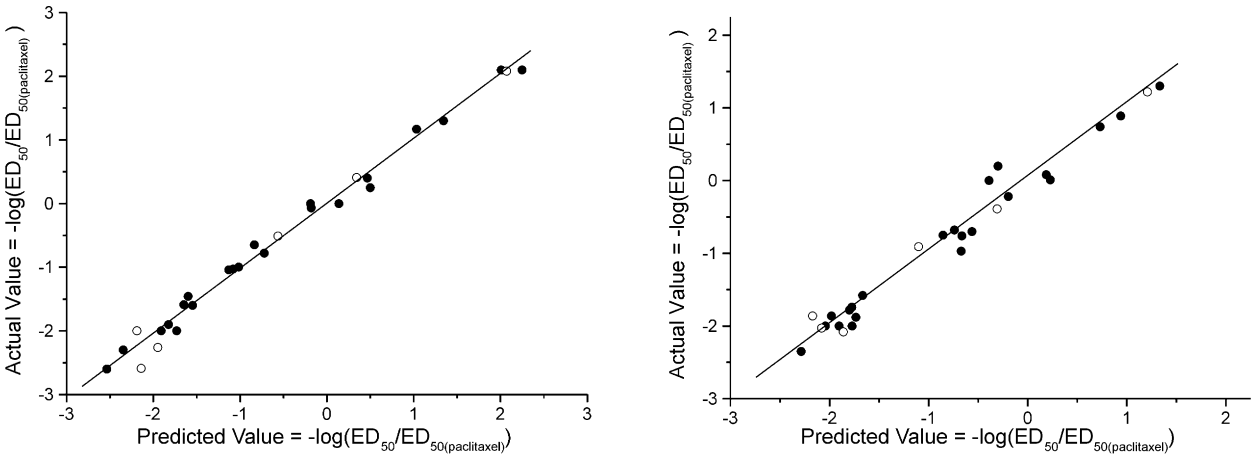

Figure 1. Predicted versus actual $-\log(ED_{50}/ED_{50(paclitaxel)})$ for the CoMFA analysis of training and test set for A549 and SK-OV-3 cell line (blank: test set, bold: training set). For A549 cell line (slope = 1.01, $r^{2*} = 0.994$) For SK-OV-3 cell line (slope:0.99, $r^{2*} = 0.986$) (* calculated on Origin 6.0).

using TMS as an internal standard. HRMS (FAB) analysis was carried out by the Mass Spectrometry Analysis Group at Korea Basic Science Institute.

Materials. The chemicals were purchased from Aldrich Co. and purified before use by standard methods. 3′-*N*-debenzoyl-3′-*N*-substituted paclitaxel analogues **1a**–**x** and **1′a–1′c** were prepared by our reported protocol:[10,19,20] 3′-*N*-(3,3′-dimethylacryloyl)-3′-*N*-debenzoylpaclitaxel (**1a**), 3′-*N*-*trans*-crotonyl-3′-*N*-debenzoylpaclitaxel (**1b**), 3′-*N*-cyclopropanecarbonyl-3′-*N*-debenzoylpaclitaxel (**1c**), 3′-*N*-cyclobutanecarbonyl-3′-*N*-debenzoylpaclitaxel (**1d**), 3′-*N*-(*p*-fluorobenzoyl)-3′-*N*-debenzoylpaclitaxel (**1e**), 3′-*N*-(*p*-nitrobenzoyl)-3′-*N*-debenzoylpaclitaxel (**1f**), 3′-*N*-(*p*-iodobenzoyl)-3′-*N*-debenzoylpaclitaxel (**1g**), 3′-*N*-(*trans*-2-methyl-2-butenoyl)-3′-*N*-debenzoylpaclitaxel (**1h**), 3′-*N*-isopropenyloxy-3′-*N*-debenzoylpaclitaxel (**1i**), 3′-*N*-(1-cyclohexenecarbonyl)-3′-*N*-debenzoylpaclitaxel (**1j**), 3′-*N*-(1-cyclopentenecarbonyl)-3′-*N*-debenzoylpaclitaxel (**1k**), 3′-*N*-vinyloxycarbonyl-3′-*N*-debenzoylpaclitaxel (**1l**), 3′-*N*-acryloyl-3′-*N*-debenzoylpaclitaxel (**1m**), 3′-*N*-(1-methyl-2-cyclohexenecarbonyl)-3′-*N*-debenzoylpaclitaxel (**1n**), 3′-*N*-(*trans*-2-pentenoyl)-3′-*N*-debenzoylpaclitaxel (**1o**), 3′ - *N* - cyclopentanecarbonyl - 3′ - *N* - debenzoylpaclitaxel (**1p**), 3′-*N*-(2-butynoyl)-3′-*N*-debenzoylpaclitaxel (**1q**), 3′-*N*-(4-pentynoyl)-3′-*N*-debenzoylpaclitaxel (**1r**), 3′-*N*-propiolyl-3′-*N*-debenzoylpaclitaxel (**1s**), 3′-*N*-phenylpropiolyl-3′-*N*-debenzoylpaclitaxel (**1t**), 3′-*N*-cyclohexanecarbonyl-3′-*N*-debenzoylpaclitaxel (**1u**), 3′-*N*-(*trans*-2-ethyl-2-hexenoyl)-3′-*N*-debenzoylpaclitaxel (**1v**), 3′-*N*-isobutyloxy-3′-*N*-debenzoylpaclitaxel (**1w**), 3′-*N*-(*trans*-2-hexenoyl)-3′-*N*-debenzoylpaclitaxel (**1x**), 3′-*N*-(3-butenyloxycarbonyl)-3′-*N*-debenzoylpaclitaxel (**1′a**), 3′-*N*-(hexyloxycarbonyl)-3′-*N*-debenzoylpaclitaxel (**1′b**) and 3′-*N*-(5-chloropentanoyl)-3′-*N*-debenzoylpaclitaxel (**1′c**).

3′-*N*-(*p*-Fluorobenzoyl)-3′-*N*-debenzoylpaclitaxel (1e). ^{1}H NMR ($CDCl_3$, selected diagnostic peaks) δ 1.06 (s, 3H), 1.18 (s, 3H), 1.60 (s, 3H), 1.71 (s, 3H), 1.81 (s, 3H), 2.29 (s, 3H), 2.19–2.25 (m, 2H), 2.15 (s, 3H), 2.42–2.50 (m, 2H), 3.72 (d, $J = 6.9$ Hz, 1H), 4.11 (d, $J = 8.4$ Hz, 1H), 4.21 (d, $J = 8.4$ Hz, 1H), 4.30 (dd, $J = 10.7$, 6.8 Hz, 1H), 4.70 (q, $J = 2.5$ Hz, 1H), 4.85 (d, $J = 8.5$ Hz, 1H), 5.58 (d, $J = 7.0$ Hz, 1H), 5.67 (dd, $J = 2.1$, 8.8 Hz, 1H), 6.14 (t, $J = 8.8$ Hz, 1H), 6.19 (s, 1H), 6.95–7.01 (m, 2H), 7.29–7.69 (m, 10H), 8.04 (d, $J = 7.4$ Hz, 2H); ^{13}C NMR ($CDCl_3$) δ 9.99, 15.20, 21.25, 22.21, 22.99, 27.24, 36.05, 43.58, 46.08, 55.51, 58.97, 72.53, 72.71, 73.53, 75.36, 75.97, 79.39, 81.57, 84.79, 116.00, 116.29, 127.43, 128.79, 129.12, 129.43, 129.58, 129.82, 129.94, 130.17, 130.21, 130.60, 133.63, 134.13, 138.32, 142.25, 166.49, 167.36, 170.79, 171.65, 173.12, 203.99; HRMS (FAB) calcd for $C_{47}H_{51}NO_{14}F$ ($M+H^+$) 872.3294, found 872.3317.

3′-*N*-(*p*-Nitrobenzoyl)-3′-*N*-debenzoylpaclitaxel (1f). ^{1}H NMR ($CDCl_3$, selected diagnostic peaks) δ 1.15 (s, 3H), 1.24 (s, 4H), 1.57 (s, 5H), 1.68 (s, 3H), 1.77 (m, 8H), 1.84–1.93 (m, 1H), 2.24 (s, 3H), 2.31 (t, $J = 8.1$ Hz, 2H), 2.38 (s, 3H), 2.45 (d, $J = 4.1$ Hz, 1H), 2.49–2.60 (m, 1H), 3.43 (d, $J = 4.8$ Hz, 1H), 3.79 (d, $J = 6.9$ Hz, 1H), 4.19 (d, $J = 8.4$ Hz, 1H), 4.32 (d, $J = 8.4$ Hz, 1H), 4.37–4.43

Table 3. In vitro anticancer activity ($-\log(ED_{50}/ED_{50(paclitaxel)})$ for test set

	Taxoid [RC(O)–]	Observed value ($-\log(ED_{50}/ED_{50(paclitaxel)})$		Predicted value ($-\log(ED_{50}/ED_{50(paclitaxel)})$	
		A549	SK-OV-3	A549	SK-OV-3
1c	Cyclopropanecarbonyl	0.41	−0.39	0.34	−0.22
1w	Isobutyloxycarbonyl	−0.51	−0.91	−0.56	−1.06
1x	*trans*-2-Hexenoyl	2.08	1.22	2.07	1.08
1′a	3-Butenyloxycarbonyl	−2.00	−1.86	−2.19	−2.17
1′b	Hexyloxycarbonyl	−2.59	−2.03	−2.14	−2.08
1′c	5-Chloropentanoyl	−2.26	−2.08	−1.95	−1.86

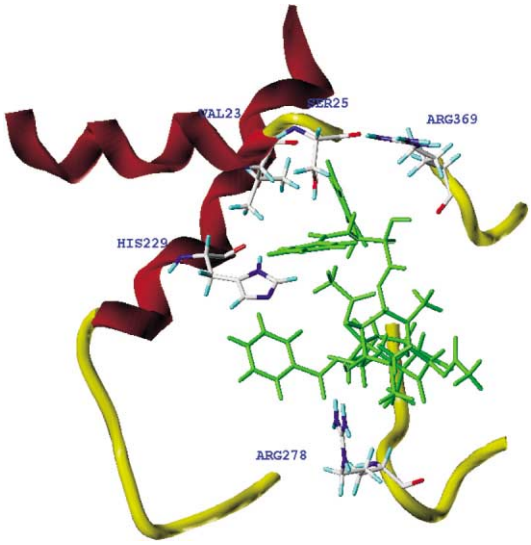

Figure 2. Binding site interactions of paclitaxel and microtubule.

(m, 1H), 4.80 (q, $J=2.4$ Hz, 1H), 4.94 (d, $J=7.9$ Hz, 1H), 5.67 (d, $J=7.0$ Hz, 1H), 5.79 (dd, $J=2.2$, 8.9 Hz, 1H), 6.21–6.27 (m, 2H), 7.09 (d, $J=8.9$ Hz, 1H), 7.36–7.65 (m, 8H), 7.90 (d, $J=8.7$ Hz, 2H), 8.13 (d, $J=8.5$ Hz, 2H), 8.24 (d, $J=8.6$ Hz, 2H); ^{13}C NMR ($CDCl_3$) δ 9.97, 14.59, 15.23, 21.26, 21.45, 22.14, 23.03, 27.29, 35.97, 36.03, 43.59, 46.07, 55.50, 59.01, 60.81, 72.57, 72.87, 73.26, 75.30, 75.91, 81.64, 84.77, 124.31, 127.46, 128.69, 129.04, 129.14, 129.49, 129.55, 130.62, 133.79, 134.21, 137.86, 139.55, 142.05, 150.23, 165.36, 167.44, 170.77, 171.66, 173.01, 203.89; HRMS (FAB) calcd for $C_{47}H_{51}N_2O_{16}$ ($M+H^+$) 899.3239, found 899.3275.

3′-*N*-Isopropenyloxy-3′-*N*-debenzoylpaclitaxel (1i). ^{1}H NMR ($CDCl_3$, selected diagnostic peaks) δ 1.15 (s, 3H), 1.26 (s, 4H), 1.59 (s, 12H), 1.68 (s, 3H), 1.80–2.04 (m, 8H), 2.36 (s, 5H), 2.49 (s, 3H), 2.52–2.63 (m, 2H), 3.33 (d, $J=5.1$ Hz, 1H), 3.79 (d, $J=7.0$ Hz, 1H), 4.18 (d, $J=8.5$ Hz, 1H), 4.29 (d, $J=8.4$ Hz, 1H), 4.35–4.42 (m, 1H), 4.51 (s, 1H), 4.64–4.68 (m, 2H), 4.94 (d, $J=7.8$ Hz, 1H), 5.29 (d, $J=8.9$ Hz, 1H), 5.68 (t, $J=9.5$ Hz, 2H), 6.28 (s, 2H), 7.39–7.61 (m, 8H), 8.09 (d, $J=7.3$ Hz, 2H);

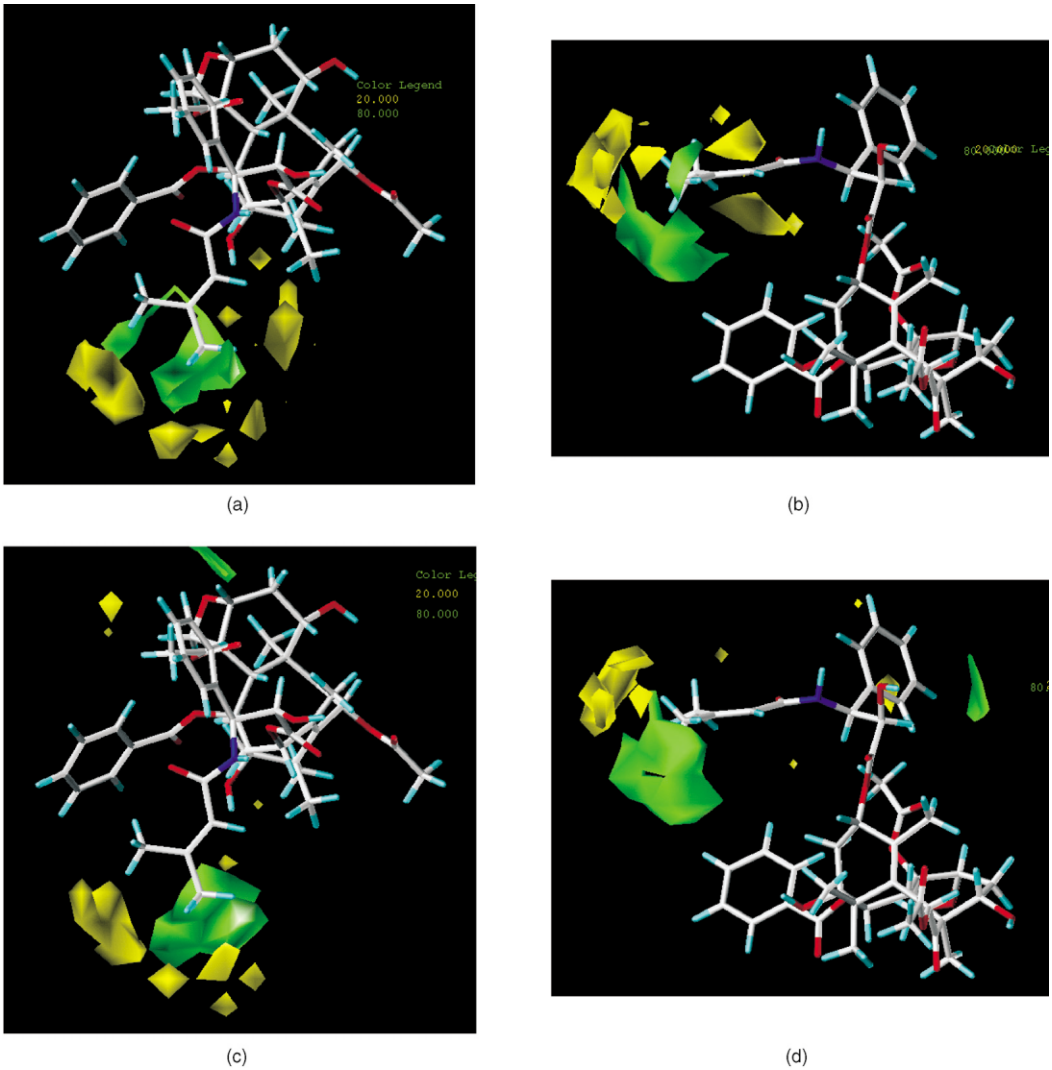

Figure 3. The steric field contour maps from the best predictive PLS analysis are plotted. Sterically favored and disfavored areas are represented by green and yellow polyhedra, respectively; A and B are for A549 cell line and top view and side view in order, C and D are for SK-OV-3 cell line and top view and side view in order. **1a** (RC(O) = 3,3′-dimethylacryloyl) is used as a reference compound.

^{13}C NMR ($CDCl_3$) δ 9.96, 15.24, 19.93, 21.24, 22.17, 22.34, 23.00, 27.22, 31.30, 35.97, 43.62, 46.04, 56.97, 59.03, 59.95, 72.56, 72.81, 73.74, 75.33, 75.96, 79.45, 79.80, 80.86, 81.20, 81.60, 84.79, 101.95, 126.54, 127.18, 128.76, 129.09, 129.37, 129.48, 130.48, 130.58, 133.63, 133.83, 134.08, 134.24, 138.19, 138.57, 142.05, 142.34, 153.07, 154.19, 157.19, 167.43, 168.78, 170.67, 171.64, 203.99; HRMS (FAB) calcd for $C_{44}H_{52}NO_{15}$ ($M+H^+$) 834.3337, found 834.3353.

3′-*N*-Vinyloxycarbonyl-3′-*N*-debenzoylpaclitaxel (1l). ^{1}H NMR ($CDCl_3$, selected diagnostic peaks) δ 1.08 (s, 4H), 1.16 (s, 6H), 1.61 (s, 6H), 1.74–1.97 (m, 5H), 2.22 (s, 6H), 2.27 (s, 2H), 2.32–2.51 (m, 2H), 3.72 (d, $J=6.87$ Hz, 1H), 4.11 (d, $J=8.4$ Hz, 1H), 4.22 (d, $J=8.3$ Hz, 1H), 4.31–4.36 (m, 1H), 4.59–4.67 (m, 2H), 4.86 (d, $J=8.5$ Hz, 1H), 5.24 (d, $J=9.1$ Hz, 1H), 5.59 (d, $J=6.9$ Hz, 1H), 5.78 (d, $J=9.3$ Hz, 1H), 6.16–6.21 (m, 2H), 6.98 (dd, $J=6.2$ Hz, 13.9 Hz, 1H), 7.27–7.55 (m, 8H), 8.03 (d, $J=7.5$ Hz, 2H); ^{13}C NMR ($CDCl_3$) δ 9.96, 15.28, 21.25, 22.20, 23.01, 27.32, 35.99, 43.58, 46.04, 56.83, 59.04, 72.59, 72.76, 73.67, 75.33, 79.54, 81.64, 84.79, 96.25, 127.21, 128.87, 129.11, 129.41, 129.52, 130.58, 133.69, 134.18, 138.08, 142.21, 153.44, 167.45, 170.74, 171.66, 172.64, 203.96; HRMS (FAB) calcd for $C_{43}H_{50}NO_{15}$ ($M+H^+$) 820.3180, found 820.3186.

3′-*N*-(4-Pentynoyl)-3′-*N*-debenzoylpaclitaxel (1r). ^{1}H NMR ($CDCl_3$, selected diagnostic peaks) δ ^{1}H NMR ($CDCl_3$, selected diagnostic peaks) δ 1.13 (s, 6H), 1.25 (s, 4H), 1.68 (s, 4H), 1.84–1.93 (m, 1H), 2.25–2.39 (m, 10H), 2.43–2.57 (m, 1H), 3.77 (d, $J=7.0$ Hz, 1H), 4.15 (d, $J=8.4$ Hz, 1H), 4.31 (d, $J=8.5$ Hz, 1H), 4.45 (m, 1H), 4.66 (d, $J=2.2$ Hz, 1H), 4.91 (d, $J=7.8$ Hz, 1H), 5.29–5.33 (m, 1H), 5.63 (d, $J=7.3$ Hz, 1H), 5.69 (d, $J=7.1$ Hz, 1H), 6.22–6.37 (m, 2H), 7.36–7.65 (m, 8H), 8.12 (d, $J=7.3$ Hz, 2H); ^{13}C NMR ($CDCl_3$) δ 9.96, 14.81, 15.62, 19.41, 20.67, 21.63, 28.76, 34.52, 34.95, 41.16, 44.23, 45.96, 46.38, 56.44, 65.16, 67.53, 69.62, 70.77, 71.69, 73.82, 75.03, 79.92, 83.02, 83.97, 85.74, 87.32, 97.82, 127.12, 128.93, 128.94, 128.97, 129.26, 130.12, 133.48, 135.82, 167.05, 170.81, 171.86, 177.92, 204.13; HRMS (FAB) calcd for $C_{45}H_{52}NO_{14}$($M+H^+$) 830.3388, found 830.3402.

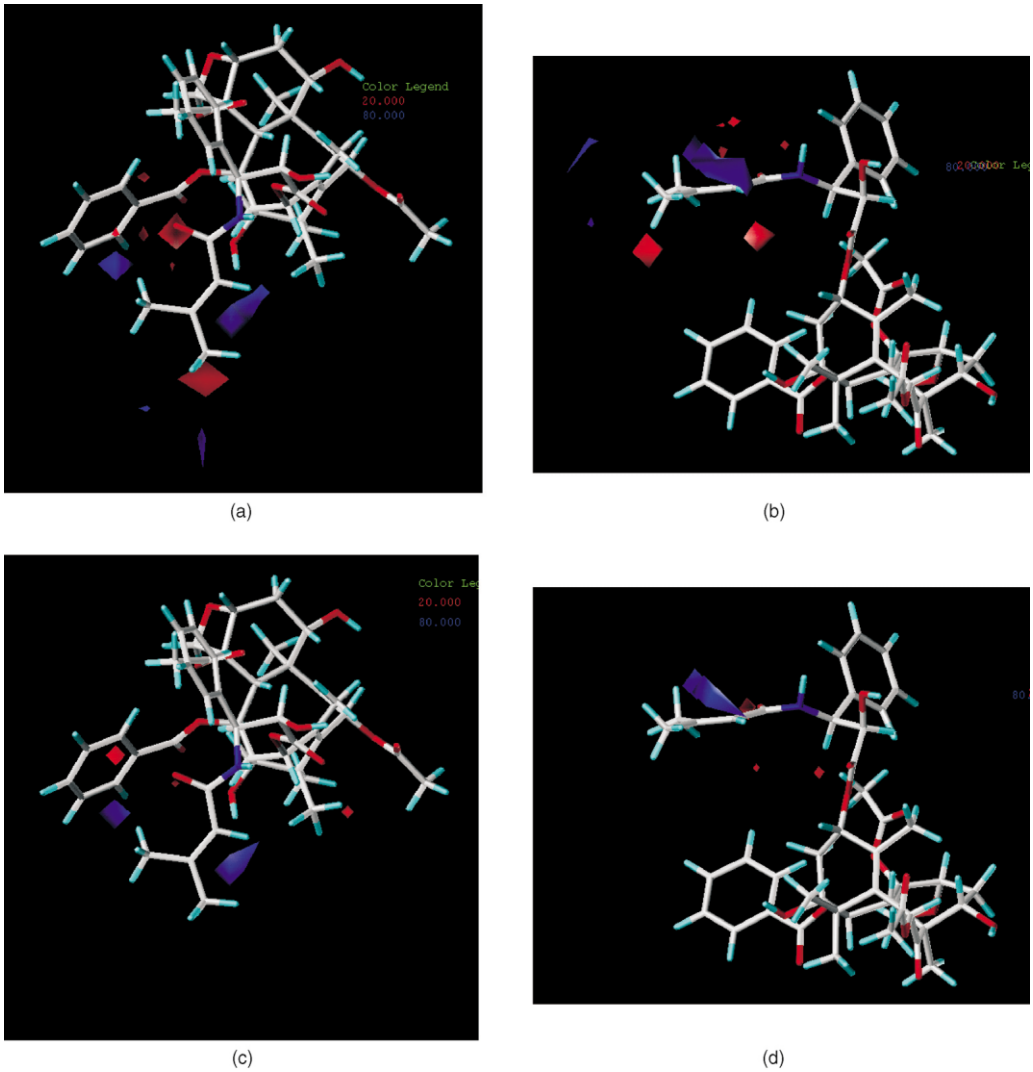

Figure 4. The electrostatic field contour maps from the best predictive PLS analysis are plotted. Blue colored regions represent that positive charge is favored and red colored regions represent that negative charge is favored; A and B are for A549 cell line and top view and side view in order, C and D are for SK-OV-3 cell line and top view and side view in order. **1a** [RC(O) = 3,3′-dimethylacryloyl] is used as a reference compound.

3′-*N*-Propiolyl-3′-*N*-debenzoylpaclitaxel (1s). ^{1}H NMR ($CDCl_3$, selected diagnostic peaks) δ 1.15 (s, 3H), 1.26 (s, 4H), 1.59 (s, 12H), 1.68 (s, 3H), 1.80–2.04 (m, 8H), 2.36 (s, 5H), 2.49 (s, 3H), 2.52–2.63 (m, 2H), 3.33 (d, J = 5.1 Hz, 1H), 3.79 (d, J = 7.0 Hz, 1H), 4.18 (d, J = 8.5 Hz, 1H), 4.29 (d, J = 8.4 Hz, 1H), 4.35–4.42 (m, 1H), 4.51 (s, 1H), 4.64–4.68 (m, 2H), 4.94 (d, J = 7.8 Hz, 1H), 5.29 (d, J = 8.9 Hz, 1H), 5.68 (t, J = 8.7 Hz, 2H), 6.28 (s, 2H), 7.39–7.61 (m, 8H), 8.09 (d, J = 7.3 Hz, 2H); ^{13}C NMR ($CDCl_3$) δ 9.52, 14.93, 20.86, 21.43, 21.89, 26.73, 35.41, 43.13, 45.54, 46.12, 47.62, 58.44, 66.26, 71.35, 72.06, 74.99, 75.51, 79.31, 80.70, 83.43, 84.37, 98.52, 127.14, 128.63, 129.03, 129.32, 130.14, 133.03, 133.91, 136.92, 142.43, 167.03, 170.02, 170.62, 171.31, 203.72; HRMS (FAB) calcd for $C_{43}H_{48}NO_{14}$ ($M+H^+$) 802.3075, found 802.3099.

3′-*N*-Isobutyloxy-3′-*N*-debenzoylpaclitaxel (1w). ^{1}H NMR ($CDCl_3$, selected diagnostic peaks) δ 0.71 (t, J = 7.8 Hz, 6H), 1.08 (s, 3H), 1.19 (s, 3H), 1.61 (s, 3H), 1.76 (s, 6H), 2.12–2.31 (m, 10H), 2.43–2.51 (m, 1H), 3.60–3.74 (m, 3H), 4.10 (d, J = 8.5 Hz, 1H), 4.22 (d, J = 8.4 Hz, 1H), 4.33 (q, J = 6.6 Hz, 1H), 4.58(s, 1H), 4.86 (d, J = 7.9 Hz, 1H), 5.22 (d, J = 8.9 Hz, 1H), 5.52–5.60 (m, 2H), 6.21 (s, 2H), 7.23–7.54 (m, 8H), 8.03 (d, J = 7.5 Hz, 2H); ^{13}C NMR ($CDCl_3$) δ 9.98, 14.59, 15.24, 19.21, 19.25, 21.25, 22.29, 27.23, 28.28, 35.95, 36.0, 56.93, 58.97, 60.80, 71.95, 72.54, 72.59, 74.03, 75.38, 75.96, 79.54, 81.54, 84.81, 127.15, 128.59, 129.09, 129.29, 129.52, 130.63, 133.51, 134.12, 138.65, 142.49, 156.71, 167.43, 170.74, 171.62, 204.03; HRMS (FAB) calcd for $C_{45}H_{56}NO_{15}$ ($M+H^+$) 850.3650, found 850.3688.

3′-*N*-(3-Butenyloxycarbonyl)-3′-*N*-debenzoylpaclitaxel (1′a). ^{1}H NMR ($CDCl_3$, selected diagnostic peaks) δ 1.15 (s, 3H), 1.27 (s, 4H), 1.68 (s, 3H), 1.83 (s, 3H), 2.25 (s, 6H), 2.37 (s, 3H), 2.53–2.58 (m, 2H), 3.42 (d, J = 5.1 Hz, 1H), 3.59–3.69 (m, 2H), 3.78–3.82 (d, J = 5.1 Hz, 1H), 3.59–3.69 (m, 2H), 3.78–3.82 (m, 2H), 3.85–3.94 (m, 1H), 4.01 (t, J = 6.6 Hz, 1H), 4.17 (d, J = 9.3 Hz, 1H), 4.29 (d, J = 8.4 Hz, 1H), 4.35–4.48 (m, 1H), 4.65 (s, 1H), 4.93–5.05 (m, 3H), 5.30 (d, J = 9.1 Hz, 1H), 5.60–5.67 (m, 3H), 6.28 (s, 2H), 7.33–7.62 (m, 8H), 8.11 (d, J = 7.4 Hz, 2H); ^{13}C NMR ($CDCl_3$) δ 9.58, 14.21, 14.91, 20.89, 21.89, 22.62, 26.86, 33.29, 35.52, 43.18, 45.62, 46.12, 56.51, 58.57, 60.44, 63.62, 64.47, 71.59, 72.19, 73.56, 74.93, 75.56, 79.17, 81.12, 84.40, 117.24, 126.74, 128.25, 128.71, 128.93, 129.08, 130.23, 133.08, 133.81, 138.12, 142.11, 156.07, 167.06, 170.35, 171.32, 172.54, 203.65; HRMS (FAB) calcd for $C_{45}H_{54}NO_{15}$ ($M+H^+$) 848.3493, found 848.3488.

3′-*N*-(Hexyloxycarbonyl)-3′-*N*-debenzoylpaclitaxel (1′b). ^{1}H NMR ($CDCl_3$, selected diagnostic peaks) δ 0.84 (t, J = 6.6 Hz, 3H), 1.15–1.29 (m, 13H), 1.49–1.51 (m, 2H), 1.68–1.71 (m, 5H), 1.83–1.93 (m, 4H), 2.19–2.34 (m, 4H), 2.38 (s, 3H), 2.49–2.58 (m, 2H), 3.35 (d, J = 4.8 Hz, 1H), 3.79 (d, J = 6.9 Hz, 1H), 3.94 (t, J = 6.7 Hz, 2H), 4.17 (d, J = 8.8 Hz, 1H), 4.30 (d, J = 8.4 Hz, 1H), 4.38–4.45 (m, 1H), 4.65 (s, 1H), 4.94 (d, J = 7.6 Hz, 1H), 5.31 (d, J = 9.4 Hz, 1H), 5.53 (d, J = 8.9 Hz, 1H), 5.66 (d, J = 7.1 Hz, 1H), 6.26–6.28 (m, 2H), 7.26–7.62 (m, 8H), 8.11 (d, J = 7.4 Hz, 2H); ^{13}C NMR ($CDCl_3$) δ 9.58, 13.99, 14.22, 14.92, 20.89, 21.09, 21.90, 22.51, 22.63, 25.33, 26.87, 28.82, 31.37, 35.51, 35.57, 43.18, 45.60, 56.46, 58.59, 60.43, 65.70, 72.22, 73.61, 74.92, 75.56, 76.61, 79.19, 81.10, 84.41, 126.75, 128.24, 128.71, 128.93, 129.05, 130.24, 133.06, 137.77, 138.19, 142.17, 156.26, 167.09, 170.35, 171.32, 172.58, 203.67; HRMS (FAB) calcd for $C_{47}H_{60}NO_{15}$ ($M+H^+$) 878.3962, found 878.3963.

3′-*N*-(5-Chloropentanoyl)-3′-*N*-debenzoylpaclitaxel (1′c). ^{1}H NMR ($CDCl_3$, selected diagnostic peaks) δ 1.15 (s, 3H), 1.27 (s, 3H), 1.68–1.72 (m, 10H), 1.82–1.91 (m, 6H), 2.21–2.35 (m, 1H), 2.49–2.54 (m, 3H), 3.43–3.45 (m, 2H), 3.52 (d, J = 4.1 Hz, 1H), 4.93 (d, J = 8.1 Hz, 1H), 5.57 (dd, J = 2.3, 8.9 Hz, 1H), 5.67 (d, J = 7.0 Hz, 1H), 6.19–6.32 (m, 3H), 7.32–7.65 (m, 8H), 8.12 (d, J = 7.3 Hz, 2H); ^{13}C NMR ($CDCl_3$) δ 9.98, 15.24, 21.27, 22.31, 23.02, 23.25,27.24, 32.17, 35.87, 35.99, 36.05, 43.62, 44.88, 46.00, 54.92, 58.98, 72.57, 72.77, 73.48, 75.35, 75.96, 79.45, 81.53, 84.79, 127.36, 128.73, 129.12, 129.41, 129.53, 130.64, 133.59, 134.14, 138.37, 142.38, 167.37, 170.67, 171.68, 172.53, 173.24, 204.05; HRMS (FAB) calcd for $C_{45}H_{55}ClNO_{14}$ ($M+H^+$) 868.3311, found 868.3316.

Molecular modelling

All molecular modeling techniques used in this research were performed with Sybyl 6.5 version on Silicon Graphics, Inc (SGI) workstations.[21]

Getting initial structure of paclitaxel. The crystallographic structure named ZETPOD[22] was selected for the initial structure of paclitaxel from Cambridge Structural Database. After modifying (7-methoxy to 7-OH), the structure was minimized with Gasteiger–Hückel charge and Tripos force field. The structures of other synthesized compounds were sketched using the minimized structure of paclitaxel by SKETCH MOLECULE and also minimized.

Constitution of training set. The presence of many rotatable bonds in paclitaxel makes various plausible conformers and the most stable conformer of paclitaxel was hard to find by grid search, systematic search and simulated annealing method implemented in Sybyl 6.5. In those circumstances, it is very time consuming and the results of calculation were diverse depending on respective conformers in training set. Therefore, the structure of docetaxel-bound microtubule[15] was used in order to select bioactive conformer of paclitaxel. The microtubule is a heterodimer consisted by α- and β-tubulin. To obtain minimized structure, α-tubulin was deleted, the complex of β-tubulin and docetaxel was minimized using the Tripos force field with Gasteiger–Hückel Charge. The position and orientation of the taxotere was assumed as same as that of paclitaxel, so the structure of docetaxel in complex was replaced by paclitaxel. And then it was also minimized using Tripos force field with Gasteiger–Hückel Charge. The result (Fig. 2) obtained from this procedure showed very similar with that obtained from Snyder's research.[23] All of the synthesized molecules were minimized by the

same procedures above. In such a way, the bioactive conformers were selected to constitute training set.

Alignment. After the bioactive conformations of all compounds were determined, the next step in CoMFA was to superimpose and align them in a three-dimensional box containing a grid by interval of each 2 and 1 Å. The superposition of the molecules is one of the most crucial steps in CoMFA, and the results of CoMFA analyses depend on this alignment of the molecules. The Atom Fit method using core backbone atoms of template structure is generally used. However, in this research, all minimized structures in training set were obtained from the active site of receptor. The alignment method based on receptor binding sites was done by Biopolymer/Fit monomers in Sybyl 6.5. In other words, the backbone atoms of paclitaxel–microtubule complex were used as a template to align the remaining analogues on microtubule complexes.

Partial least-squares analysis. To find the optimum number of principal components corresponding to the smallest error of prediction, a 'leave-one-out' cross-validation procedure was performed. To obtain better r^2_{cv} and shorten analysis time, the column filtering value was assigned. In other words, weak descriptors lower than defined column filtering values ($0.5 \sim 2.0$ kcal mol^{-1} were defined) were deleted and then PLS analyses[24] were performed. During the PLS analyses, Region Focusing method was also used. Region focusing is the application method to distinguish the lattice points in a CoMFA region depending on the contribution of those points to subsequent analyses in order to increase signal-to-noise in analysis. First, we began two grid spacings—2 and 1 Å—and then the resolution of the former was increased to 1 Å grid interval and the one of the latter was to 1 Å grid interval during the process of region focusing. StDev*Coefficients, Discriminant Power and Modeling Power were used as weighting contributors. The sharpness of focusing was controlled by exponential factors; 0.3 and 0.5. From the above process we got various CoMFA regions of which grid interval was tighter and finer than the default one (2 Å) and of which grid interval was finer than that of 1 Å. These intervals were used in conjunction with the column filtering values to make PLS calculations at much finer grid resolution.

Cytotoxicity assay

Materials and methods. The human non-small cell lung cancer cell line A549 and the ovarian cancer cell line SK-OV-3 were used in this study. The cells were grown in RPMI1640 medium supplied with 5% fetal bovine serum (FBS) and cultured in a 95% air/5% CO_2 atmosphere at 37 °C in a humidified incubator, and the cells were dissociated with 0.25% trypsin and 3 mM EDTA in phosphate buffered solution in case of transferring or dispensing before experiment.

Growth inhibition assay and data analysis. All experimental procedures followed the NCI's protocol with some minor changes based on the SRB method as described previously.[11,12] Briefly, after 72 h of continuous drug-expose time, the cells were fixed with 10% cold TCA, followed by staining with 0.4% SRB solution. Then, the cells were washed, and the cell membrane-bound stains were solubilized with 10 mM unbuffered Trisma base solution (pH 10.5). The value of optical density (OD value) was measured spectrophotometrically at 520 and 690 nm in a microtiter plate reader (Molecular Devices E-max, Sunnyvale, CA, USA), and the OD value at 690 nm was subtracted from that at 520 nm so as to eliminate the effects of non-specific absorbance. Cell survival fractions were calculated with the aid of three basic measurements; a time zero (T_z) at the beginning of drug incubation, a cell control (CC) at the end of incubation without drug, and a drug-treatment (DT) at the end of the drug incubation period. If $DT \geq T_z$, the net percent of cell growth inhibition was calculated by $(DT-T_z)/(CC-T_z)\times 100$. If $DT < T_z$, the net percent of cell killing activity was calculated by $(DT-T_z)/T_z\times 100$. All the data represented the average values of three wells in each experiment.

Acknowledgements

Financial support from the Ministry of Science and Technology of Korea (2N16490 and 2N22890 to C. E. Song) is gratefully acknowledged.

References and Notes

1. Wani, M. C.; Taylor, H. L.; Wall, M. E.; Coggon, P.; Mcphail, A. T. *J. Am. Chem. Soc.* **1971**, *93*, 2325.
2. Schiff, P. B.; Fant, J.; Horwitz, S. B. *Nature* **1979**, *277*, 665.
3. Manfredi, J. J.; Horwitz, S. B. *Pharmacol. Ther.* **1984**, *25*, 83.
4. Ringel, I.; Horwitz, S. B. *J. Natl. Cancer Inst.* **1991**, *83*, 288.
5. Rowinski, E. K.; Donehower, R. C. *Pharmacol. Ther.* **1991**, *52*, 35.
6. Verweij, J.; Clavel, M.; Chevalier, B. *Ann. Oncol.* **1994**, *5*, 495.
7. Georg, G. I., Chen, T. T., Ojima, I., Vyas, D. M., Ed. In *Taxane Anticancer Agents: Basic Science and Current Status*; ACS Symposium Series 583; American Chemical Society: Washington, DC, 1995; pp 189, 203, 217, 247, 262.
8. Georg, G. I.; Boge, T. C.; Cheruvallath, Z. S.; Clwers, J. S.; Harriman, G. C. B.; Hepperle, M.; Park, H. In *Taxol®*: Science and Applications; Suffness, M. Ed.; CRC: New York, 1995, p 317.
9. (a) Nicolaou, K. C.; Dai, W.-M.; Guy, R. K. *Angew. Chem. Intl. Ed. Engl.* **1994**, *33*, 15. (b) Kingston, D. G. I. *Pharmacol. Ther.* **1991**, *52*, 1.
10. Roh, E. J.; Song, C. E.; Kim, D.; Pae, H.-O.; Chung, H.-T.; Lee, K. S.; Chai, K.; Lee, C. O.; Choi, S. U. *Bioorg. Med. Chem.* **1999**, *7*, 2115.
11. Skehan, P.; Storeng, R.; Scudiero, D.; Monks, A.; McMahon, J.; Vistica, D.; Warren, J. T.; Bokesch, H.; Kenney, S.; Boyd, M. R. *J. Natl. Cancer Inst.* **1990**, *82*, 1107.
12. Choi, S.-U.; Lee, C.-O.; Kim, K.-H.; Choi, E.-J.; Park, S.-H.; Shin, H.-S.; Yoo, S.-E.; Jung, N.-P.; Lee, B.-H. *Anti-Cancer Drugs* **1998**, *9*, 157.
13. (a) Cramer, R. D.; Patterson, D. E.; Bunce, J. D. *J. Am. Chem. Soc.* **1988**, *110*, 5959. (b) Cramer, R. D.; Depriest, S. A.; Patterson, D. E.; Hecht, P. 3-D QSAR. In *Drug Design. Theory, Methods and Applications*; Kubinyi, H. Ed.; Escom: Leiden; p 443.

14. (a) Waller, C. L.; Oprea, T. I.; Giolitti, A.; Marshall, G. R. *J. Med. Chem.* **1993**, *36*, 4152. (b) De Priest, S. A.; Mayer, D.; Naylor, C. B.; Marshall, G. R. *J. Am. Chem. Soc.* **1993**, *115*, 5372. (c) Cho, S. J.; Garsia, M. L.; Bier, J.; Tropsha, A. *J. Med. Chem.* **1996**, *39*, 5064. (d) Vaz, R. J.; McLean, L. R.; Pelton, J. T. *J. Comput.-Aided Mol. Des.* **1998**, *12*, 99. (e) Pastor, M.; Cruciani, G.; Watson, K. *J. Med. Chem.* **1997**, *40*, 4089.
15. Nogales, E.; Wolf, S. G.; Downing, K. H. *Nature* **1998**, *391*, 199.
16. Lindgren, F.; Geladi, P.; Rännar, S.; Wold, S. *J. Chemometrics* **1994**, *8*, 349.
17. Oprea, T. I.; Garcia, A. E. J. *Comput.-Aided Mol. Design* **1996**, *10*, 186.
18. Gueritte-Voegelein, F.; Guenard, D.; Lavelle, F.; Le Goff, M-T.; Mangatal, L.; Potier, P. *J. Med. Chem.* **1991**, *34*, 992.
19. Roh, E. J.; Park, Y. H.; Song, C. E.; Oh, S.; Choe, Y. S.; Kim, B.; Chi, D. Y.; Kim, D. *Bioorg. Med. Chem.* **2000**, *8*, 65.
20. Roh, E. J.; Kim, D.; Lee, C. O.; Song, C. E. *Bioorg. Med. Chem.* **2002**, *10*, in press.
21. SYBYL 6.5; Tripos Associates, Inc.: St. Louis, MO, USA
22. (a) Cambridge Crystallographic Data Centre (CCDC), 12 Union Road, Cambridge CB2 1EZ, UK. (b) Mastropaolo, D.; Camerman, A.; Luo, Y.; Brayer, G. D.; Camerman, N. *Proc. Nat. Acad. Sci. USA* **1995**, *92*, 6920.
23. Snyder, J. P.; Nettles, J. H.; Cornett, B.; Downing, K. H.; Nogales, E. *Proc. Natl. Acad. Sci. U.S.A.* **2001**, *98*, 5312.
24. (a) Wold, S.; Ruhe, A.; Wold, H.; Dunn, W. J. *SIAM J. Sci. Stat. Comput.* **1984**, *5*, 735. (b) Lorber, A.; Wangen, L. E.; Kowalski, B. R. *J. Chemometrics* **1987**, *1*, 19. (c) Hoskuldsson, A. *J. Chemometrics* **1988**, *2*, 211.